Koichi Nishimura, MD • Masanori Kitaichi, MD • Takateru Izumi, MD • Sonoko Nagai, MD
Masaki Kanaoka, MD • Harumi Itoh, MD

Usual Interstitial Pneumonia: Histologic Correlation with High-Resolution CT[1]

The authors reviewed 46 cases of idiopathic pulmonary fibrosis with usual interstitial pneumonia (UIP), correlating findings on high-resolution computed tomographic (HRCT) scans with findings in specimens obtained at open lung biopsy and autopsy. The following HRCT findings were observed: (*a*) an accumulation of small cystic spaces with thick walls, (*b*) air bronchiolograms within areas of intense lung attenuation, (*c*) rugged pleural surfaces, (*d*) irregularly thickened pulmonary vessels, (*e*) bronchial wall thickening, and (*f*) slightly increased lung attenuation. Macroscopic honeycombing correlating with small cystic spaces was demonstrated at HRCT and pathologic examination. Air bronchiolograms in the areas of intense lung attenuation (ie, microscopic honeycombing) corresponded to dilated bronchioles (> 1 mm in diameter) with fibrosis. Irregularly thickened vessels and bronchial walls and irregular pleural surfaces were the result of fibrosis in the periphery of the secondary pulmonary lobules. Areas of slightly increased lung attenuation seen on the HRCT scans correlated with patchy alveolar septal fibrosis or inflammation. The authors conclude that microscopic honeycombing and a perilobular distribution in UIP may be clearly identified with HRCT.

Index terms: Computed tomography (CT), high-resolution, 60.1211 • Lung, CT, 60.1211 • Lung, fibrosis, 60.79 • Pneumonitis, usual interstitial, 60.79

Radiology 1992; 182:337–342

[1] From the Chest Disease Research Institute, Kyoto University, Sakyo-ku, Kyoto 606, Japan, and the Department of Radiology and Nuclear Medicine, Kyoto University Hospital, Kyoto, Japan. Received September 10, 1990; revision requested October 16; final revision received September 10, 1991; accepted September 23. **Address reprint requests to** K.N.

THERE have been reports on the application of computed tomography (CT) in evaluation of peripheral pulmonary lesions in diffuse infiltrative lung diseases (1–3). In some cases, high-resolution computed tomography (HRCT) has been used (4,5). Mathieson et al reported that CT was superior to chest radiography for specific diagnosis in 118 patients with chronic diffuse infiltrative lung disorders (6). However, there have been only a limited number of studies correlating findings at CT with findings at pathologic examination. Findings in recently published articles have shown that secondary pulmonary lobules can be identified with HRCT (7–11). Murata et al reported that use of HRCT enables classification of pulmonary parenchymal disease into centrilobular, panlobular, bronchovascular, and perilobular distributions (12).

Idiopathic pulmonary fibrosis, found relatively frequently among diffuse infiltrative lung disorders, has a progressive course. There are two histologic forms of idiopathic pulmonary fibrosis: usual interstitial pneumonia (UIP) and desquamative interstitial pneumonia. Many investigators believe, however, that UIP and desquamative interstitial pneumonia represent different stages of the same disease (13,14). Several articles have been published that describe CT-pathologic correlations in idiopathic pulmonary fibrosis. Müller et al described three main patterns of CT findings for idiopathic pulmonary fibrosis: a reticular pattern, honeycombing, and areas of air-space opacification (ground-glass opacities) (7,15,16). Pathologically, the reticular pattern corresponded to irregular fibrosis or small (< 5 mm) cystic spaces, and the honeycombing corresponded to cystic spaces that were 2–20 mm in diameter. The areas of air-space opacification corresponded to areas of active alveolitis. These data are based on findings in a limited number of patients, and the authors did not assess the distribution of abnormalities in relation to the secondary pulmonary lobules. Westcott and Cole reported that traction bronchiectasis was found with standard CT scanning in end-stage pulmonary fibrosis (17).

To evaluate further the early findings of UIP with HRCT, we performed correlative studies between findings on HRCT scans and findings in inflated specimens obtained at open lung biopsy and autopsy in 46 patients with idiopathic pulmonary fibrosis.

MATERIALS AND METHODS

CT scanning was performed with a model T8800 scanner (GE Medical Systems, Milwaukee) with 5-mm collimation, while patients held their breath for 9.6 seconds at deep end-inspiration. A high-spatial-resolution algorithm (bone algorithm) was used to analyze the CT scans of all the patients. Scans were obtained with HRCT at a window level appropriate for pulmonary parenchyma (−800 HU) and a width of 1,000 HU. The mediastinum, hilum, and chest wall were observed at a window level appropriate for soft tissue (0 HU) and a width of 250 HU.

By using the criteria described by Carrington et al (13), the histologic diagnosis of UIP was confirmed with an open lung biopsy in 46 patients. In all patients, the diagnosis was idiopathic UIP, that is, idiopathic pulmonary fibrosis (14). The patients consisted of 36 men and 10 women, who ranged in age from 42 to 71 years (mean, 58.2 years ± 7.9). Eighteen patients were current smokers; 17 were former smokers; and 11 had never smoked. Shortness of breath that had been present for 12 months or less was reported in 16 cases, for 2–3 years in 10 cases, and for over 4 years in eight cases. Ten patients were asymptomatic but were referred for CT

Abbreviations: HRCT = high-resolution CT, UIP = usual interstitial pneumonia.

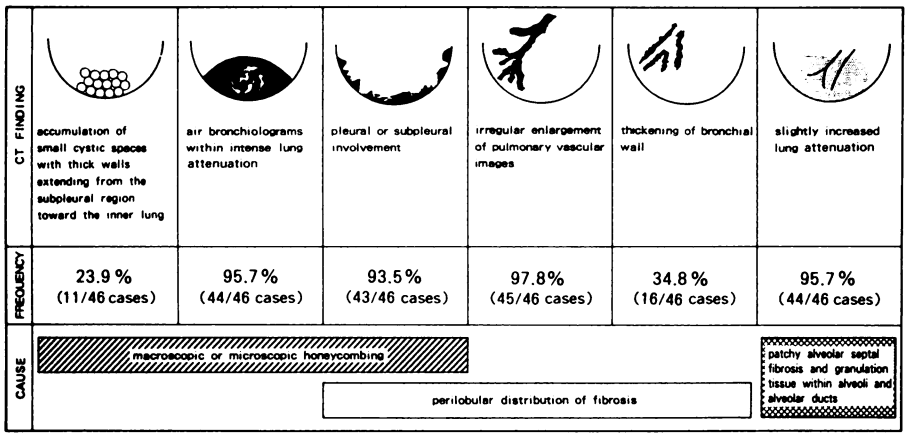

Figure 1. Schematic representation of the HRCT findings in UIP.

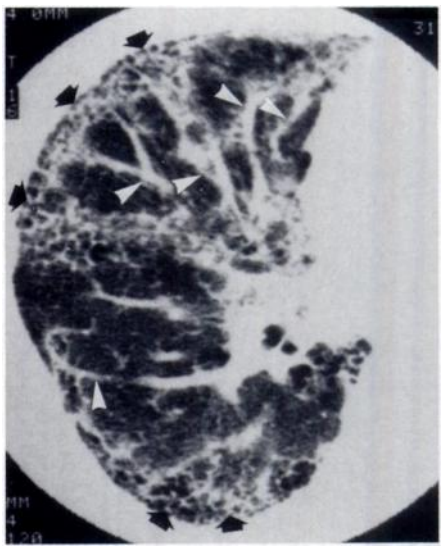

Figure 2. HRCT image shows accumulated small cystic lesions with thick walls (arrows) and irregularly thickened bronchovascular bundles (arrowheads). These CT findings are representative of UIP in our series.

scanning because of abnormal findings on chest radiographs that had been obtained during routine examinations. Two patients complained of a cough without shortness of breath. HRCT images of 13 patients were obtained within a week prior to biopsy; the period from CT to open biopsy was 2–94 days (mean, 28.1 days). The patients were clinically stable prior to both CT and the biopsy procedure; no deterioration in findings on chest radiographs was observed in any case during the period between CT and biopsy.

Open lung biopsy was performed on the left lung of 29 patients and on the right lung of 17. Biopsy samples were obtained from two or three different lobes; three biopsy specimens were obtained in nine cases, and two specimens were obtained in 37. Each specimen obtained from open biopsy was inflated and fixed with multiple injections of formaldehyde solution by using a transpleurally inserted 26.5-gauge needle. Specimens were stained with hematoxylin-eosin stain and the Weigert method for elastic fibers. After fixation, sliced specimens were observed with a stereomicroscope. Histologic findings under low magnification were compared with findings on the prebiopsy HRCT images of the biopsy site. To obtain a rigorous CT-pathologic correlation, one radiologist (M.K. or H.I.) and one pathologist (M.K.) observed the lung macroscopically during thoracotomy and recorded the site from which each biopsy specimen was taken. These stereomicroscopic findings were of assistance in correlation of findings in histologic studies with those on HRCT images.

Although lung cancer was found during biopsy in three cases and hamartoma was found in one, these neoplastic lesions were all resectable. After biopsy had been performed, lung cancer developed in two patients, laryngeal cancer in one, and carcinoma of the gallbladder in one. Thirteen of the 46 patients have subsequently died. Three patients died of cancer 8–29 months after biopsy, and 10 patients died of progressive respiratory failure 1–34 months (mean, 15.6 months) after biopsy.

Autopsies were performed on four patients who died of progressive respiratory failure and on two patients who died of lung cancer. To inflate and fix the lungs in these cases, a solution containing formaldehyde and polyethylene glycol, as described by Heitzman, was injected into the bronchus of either the right or left lung (18). After the solution was removed and the lungs were dried, the lungs were sliced into either 1- or 5-mm-thick sections and contact radiographs of each specimen were made. The stereomicroscopic and histologic findings were studied and compared with findings on HRCT scans obtained while the patient was alive. Subsequently, comparisons were made of findings on the contact radiographs and on the HRCT scans with findings from the stereomicroscopic and histologic examinations of inflated and sliced lungs.

RESULTS

The major HRCT findings for the 46 UIP cases were as follows (Figs 1, 2): (*a*) an accumulation of cystic spaces greater than 5 mm in diameter that have thick walls and extend from the subpleural region toward the inner lung (n = 11 [23.9%]); (*b*) air bronchiolograms within areas of intense lung attenuation (n = 44 [95.7%]); (*c*) rugged pleural surfaces or pleural or subpleural involvement (n = 43 [93.5%]); (*d*) irregular enlargement of the pulmonary vessels (n = 45 [97.8%]); (*e*) thickening of the bronchial wall (n = 16 [34.8%]); and (*f*) slightly increased lung attenuation (n = 44 [95.7%]).

In the four cases in which the lungs were inflated and fixed post mortem, it was clearly evident that the accumulated cystic lesions depicted on the HRCT images represented gross honeycombing. The presence of 1–2-mm-diameter air bronchiolograms at HRCT suggested that the peripheral airways were dilated in the regions with markedly increased lung attenuation (Fig 3). In the corresponding biopsy specimens, 1–2-mm-diameter dilated bronchioles were surrounded by airless fibrotic lung tissue. These areas of mild bronchiolar dilatation with surrounding fibrosis had the same histologic findings as those of the gross honeycombing lesions. Therefore, the term "microscopic honeycombing" was used. Dilated bronchioles leading toward the area of microscopic honeycombing were sometimes filled with mucinous secretions, perhaps accounting for some occasional indistinctness of air bronchiolograms within regions of high attenuation.

In HRCT scans, apparent enlargement of the vascular structure was observed along the relatively large vessels, including both pulmonary arteries and veins (Fig 4). Histologically, dilatation of the vessels themselves was not detected in biopsy or autopsy specimens. Although the walls of the bronchi were seldom thickened, the walls of the large airways often seemed to be thickened. Apparent thickening of vessels and bronchial walls was the result of fibrosis in the lung tissue surrounding the vessels and airways. Subpleural areas were also affected by fibrotic changes in UIP, which resulted in the appearance of a rugged pleural surface on the HRCT images (Fig 5). Indeed, these three HRCT findings—thickened vessels and bronchial walls and subpleural involvement—seemed to be caused by the tendency for fibrosis to occur in the periphery of the secondary pulmonary lobule (Fig 6).

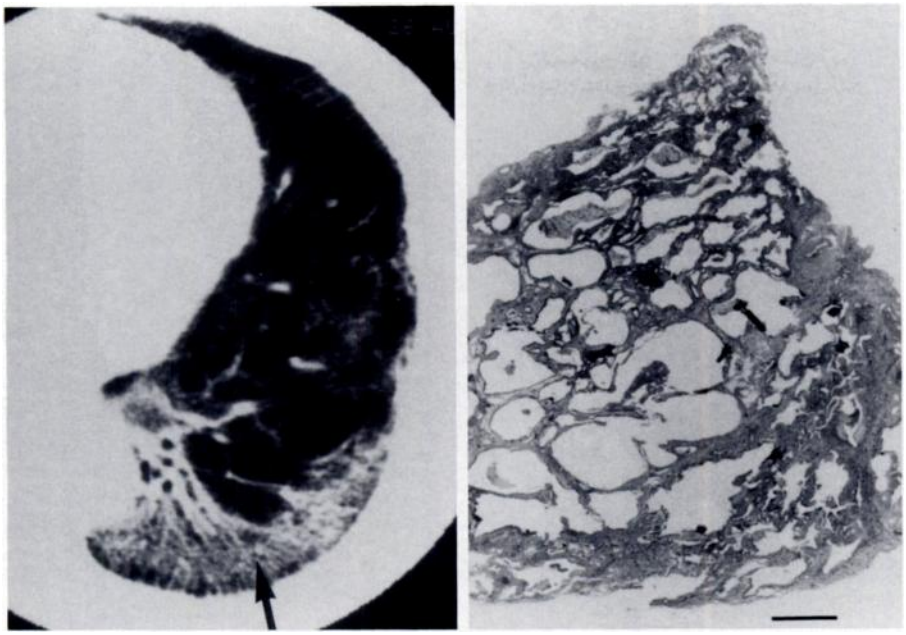

a. b.

Figure 3. **(a)** Air bronchiolograms within area of high attenuation are seen in UIP at HRCT. **(b)** Lung section of a biopsy sample corresponds to area in **a.** Bronchioles are dilated about 1 mm in diameter and are surrounded by fibrotic walls; this is termed microscopic honeycombing. This specimen was obtained from the left lower lobe (segment 6), as shown by the arrow in **a.** Scale indicates 1 mm.

Focal areas of slightly increased attenuation of lung parenchyma were also identified (Fig 7). This HRCT finding in UIP often had ill-defined boundaries with normal lung parenchyma. Histologic sections taken from the affected regions demonstrated an uneven distribution of areas of fibrosis interspersed with relatively normal alveoli.

The main histopathologic finding in the four lungs examined post mortem from patients who died of progressive disease was diffuse alveolar damage associated with UIP (19). Contact radiographs of the sliced lungs showed that x-ray transmission was severely limited in even mildly involved areas. Diffuse alveolar damage was seen throughout the peripheral lung. Since diffuse alveolar damage was not identified in any biopsy specimens from UIP cases, it may be that just prior to death, widespread diffuse alveolar damage obscured the findings of UIP. It was therefore difficult to perform a correlative study examining lungs post mortem for findings such as patchy interstitial cellular infiltrates and fibrosis, findings that would be consistent with UIP.

At HRCT, small, low-attenuation areas and/or large, subpleural cystic areas were depicted in 15 of the 46 cases (Fig 7). These areas, distributed in the upper lung zones and not associated with thick walls, were distinct from the accumulated small cystic lesions and most likely represented areas of emphysema.

High-attenuation nodular areas were seldom identified with CT in cases of UIP. However, in three patients, CT did reveal high-attenuation nodules that were not appreciated on chest radiographs. These lesions were confirmed to represent lung cancer and were completely resected at thoracotomy: Two proved to be localized adenocarcinomas, and the other was an epidermoid carcinoma.

DISCUSSION

To optimize the clinical usefulness of HRCT, it is necessary to elucidate the pathologic features corresponding to each CT finding. In a study examining the correlation between the findings on a standard CT scan and those at pathologic examination of lungs post mortem, Müller et al determined that honeycombing with a diameter of more than 2 mm could be seen as a reticular pattern on CT images (15). In addition, Westcott and Cole have reported that traction bronchiectasis represents a pathologic feature of the honeycombing that may be appreciated on both plain radiographs and CT scans (17). In our study, bronchiolar dilatation of about 1 mm in diameter was associated with the surrounding fibrosis; that is, microscopic honeycombing could be visualized on the HRCT scans (Fig 3). Such microscopic honeycombing may not be manifested as typical cysts but rather as air bronchiolograms within areas of high attenuation. Routine radiography of the areas with histologically proved microscopic honeycombing did not reveal any coarse reticular or oval shadows, as were described by Heitzman for gross (macroscopic) honeycombing (18).

In the initial studies of CT scanning of pulmonary parenchyma, the standard algorithm was used instead of the bone-detail algorithm, with 1-cm collimation. Use of the bone-detail algorithm may make it possible to visualize even microscopic honeycombing with a diameter of about 1 mm. Although Todo and Herman reported the use of HRCT with 5-mm collimation (9), recent studies with HRCT of pulmonary parenchyma have used 1.5-mm collimation. However, we used 5-mm collimation in the study presented herein to depict the apparent vessels on each image, which serve as landmarks for the identification of the secondary pulmonary lobules. Nevertheless, the use of 1–2-mm collimation in conjunction with the bone-detail algorithm may allow visualization of finer structures in the pulmonary parenchyma.

Weibel has divided the interstitium into three compartments: axial, parenchymal, and peripheral (20). Similarly, Bergin and Müller have classified the distribution of interstitial diseases as depicted at CT into three categories: axial, middle, and peripheral (2,3). Bergin and Müller (2,3) and Wright et al (21) have noted that UIP is marked by a peripheral distribution on CT scans. Results from the study presented herein closely parallel these observations. However, our findings of thickened vessels and bronchial walls at HRCT scanning also demonstrate an axial distribution.

Fibrotic lesions in UIP are often located in the periphery of the secondary pulmonary lobules, adjacent to interlobular septa. This distribution has been classified as perilobular by Murata et al (12). In the subpleural area, secondary pulmonary lobules are bordered by well-developed interlobular septa and pleura. Subpleural fibrosis at the periphery of the secondary pulmonary lobules seems to account for the rugged pleural surfaces seen on the HRCT scans (Fig 5). In the more central portion of the lung, secondary pulmonary lobules are bordered by extralobular pulmonary vessels and bronchi (5). Vessels

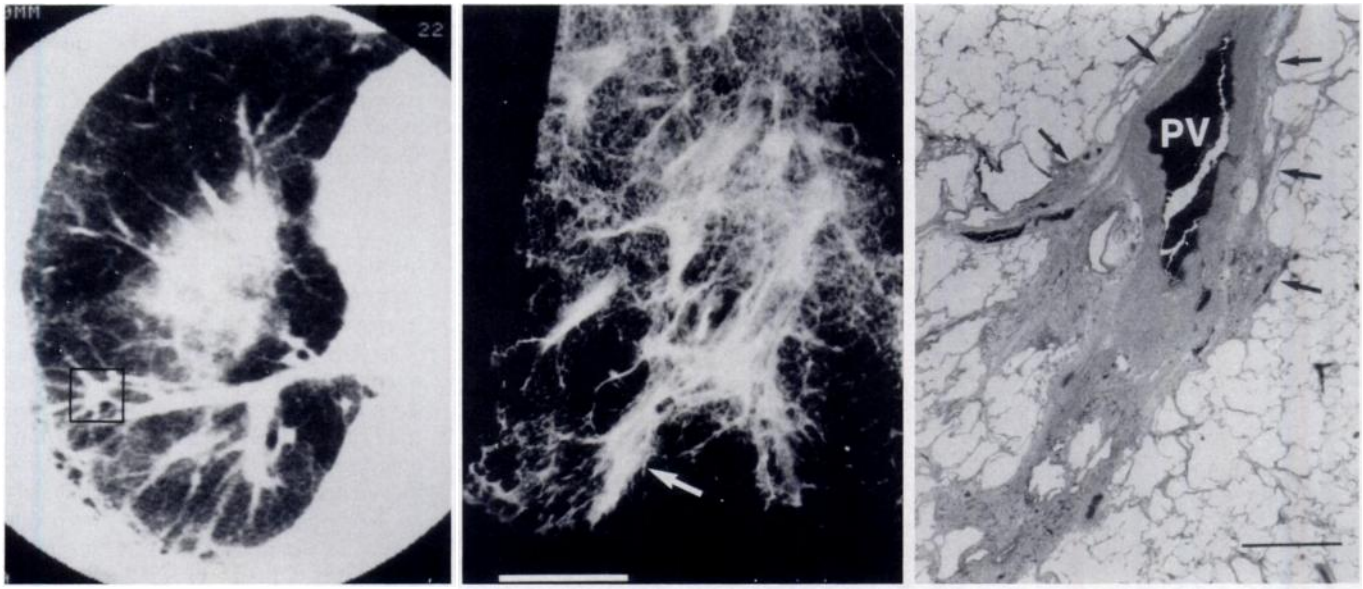

a. b. c.

Figure 4. **(a)** Irregularly enlarged pulmonary vessels are seen in UIP. **(b)** Contact radiograph of a thin slice of lung was obtained post mortem from the boxed area in **a.** Lung cancer developed after biopsy in this case. An autopsy was performed 8 months after the biopsy. The right lung was fixed post mortem by using a solution described by Heitzman (18). Note that the bronchovascular bundles are irregularly thickened. Scale indicates 1 cm. **(c)** Lung section of specimen was obtained from the area shown by the arrow in **b.** The pulmonary vein is surrounded by perilobular fibrotic lesions (arrows). Scale indicates 1 mm. *PV* = pulmonary vein.

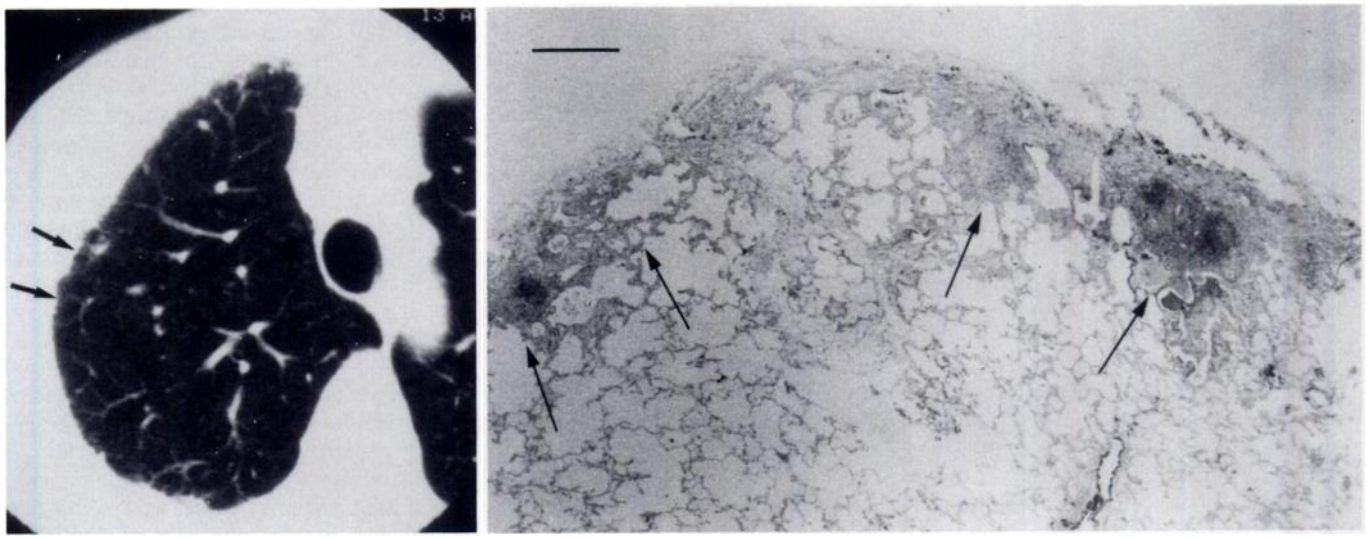

a. b.

Figure 5. **(a)** Rugged pleural surface and pleural or subpleural involvement are seen in UIP (arrows). **(b)** Lung section of a biopsy sample corresponds to area in **a.** While fibrotic lesions are apparent in the subpleural area (arrows) about 1 mm from the pleural surface, alveoli in the inner parts are almost normal in appearance. This subpleural involvement is another finding suggestive of a perilobular distribution. This specimen was obtained in and around the area indicated by the arrows in **a,** from the right upper lobe (segment 1). Scale indicates 1 mm.

may appear to be prominent because of the presence of intraluminal, intramural, or perivascular lesions or because of the presence of other abnormalities within the surrounding lung tissues. In UIP, the apparent enlargement of vascular structures seen on HRCT scans is probably the result of fibrotic changes that occur adjacent to vessels (Fig 4). Similarly, thickened bronchial walls are most likely the result of bronchial fibrosis that is also located in the peripheral regions of the adjacent secondary lobules. The histologically perilobular location of lesions accounts for their apparent axial arrangement on HRCT scans (Fig 6).

Staples et al reported that interstitial fibrosis may be manifested by a finely irregular interface of pleura, vessels, or bronchi with normal lung parenchyma and by the established findings of reticular markings and cystic spaces (22). The findings in the study presented herein are in agreement with these observations. These thickened vessels and bronchial walls may be similar to the thickened bronchovascular bundles reported previously (23). Bergin et al reported that although bronchovascular bundle thickening seen on CT scans is marked in cases of sarcoidosis and lymphangitic carcinomatosis, such thickening is only sparse and mild in cases of UIP (24). While the bronchovascular sheath itself is originally affected in cases of both sarcoidosis and

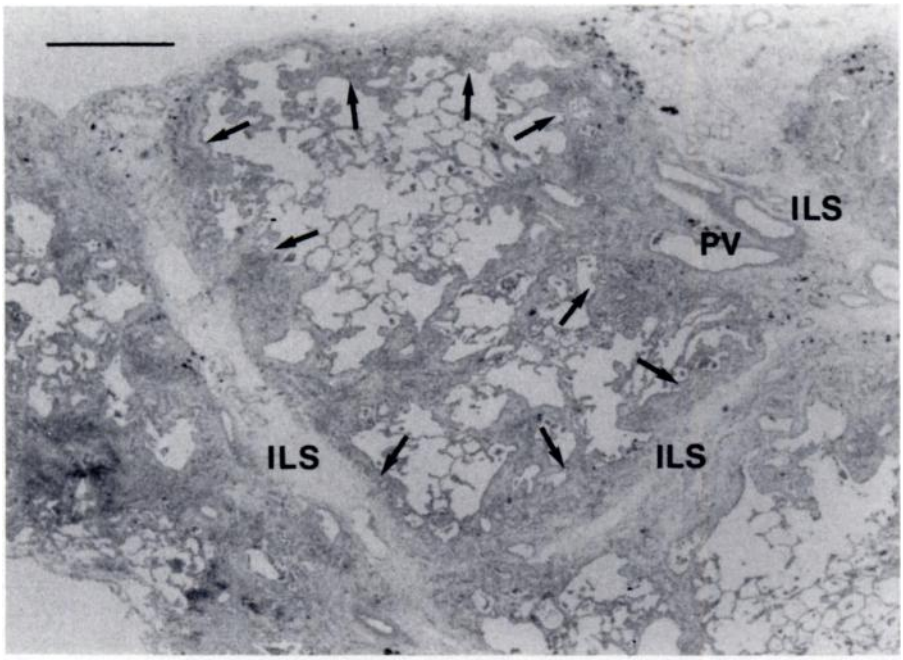

Figure 6. Representative lung section shows a perilobular distribution in UIP. A whole lobule is bordered by interlobular connective tissue. Fibrotic lesions are distributed perilobularly (arrows). The pulmonary veins located adjacent to interlobular septa are surrounded by fibrotic lesions. Scale indicates 1 mm. *ILS* = interlobular septum, *PV* = pulmonary vein.

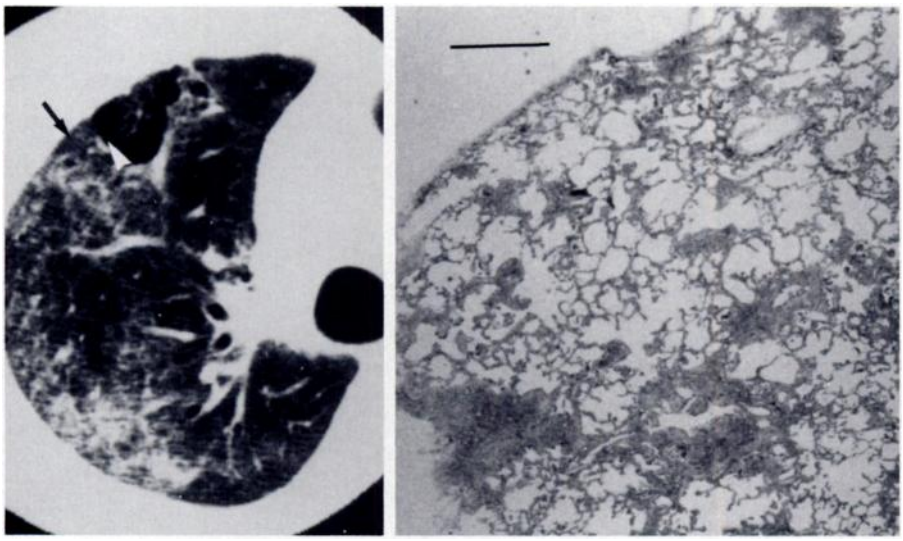

a. **b.**

Figure 7. **(a)** Slightly increased lung attenuation (arrow) and subpleural bullous region (arrowhead) are seen in UIP. The inner vascular and linear structures are visible within the area with slightly increased attenuation. **(b)** Lung section of a biopsy sample corresponds to area in **a.** Although some alveolar septa are fibrous and thickened by cell infiltration without honeycombing, others are almost normal. Histologically, patchy involvement is observed within a secondary lobule. Terminal air spaces are partially preserved so that the attenuation of this area is slightly increased on the corresponding HRCT image. This specimen was obtained from the right upper lobe (segment 3), as indicated by the arrow in **a.** Scale indicates 1 mm.

lymphangitic carcinomatosis (23,25), we observed that the lesions are distributed mainly along the alveolar walls adjacent to the sheaths in UIP (Fig 6).

Patchy distribution is one of the fundamental histologic findings in the diagnosis of UIP; some alveolar walls may be spared, even within an involved secondary lobule (13). In areas of slightly increased attenuation on the HRCT scans, a heterogeneous distribution of lesions within the secondary pulmonary lobules may explain why the boundaries with the normal lung may be unclear (Fig 7). If the whole lobule is homogeneously involved (ie, in a panlobular distribution), then sharply demarcated areas of increased attenuation will be found on the HRCT scans (12).

It has been suggested that alveolitis represents an early phase of UIP (14). It is possible that alveolitis may be present in areas of slightly increased attenuation, and, although the slightly increased lung attenuation may be less remarkable, it should not be overlooked (Fig 7). Müller et al reported that opacification of the air spaces was seen better with 1.5-mm collimation than with 10-mm collimation and that disease activity could be estimated by means of CT scanning. A high pathologic score for disease activity, suggestive of alveolar cellular desquamation and alveolar septal inflammation, was markedly associated with high CT scores for opacification of air space (16). However, it is possible that the slightly increased attenuation in the lung was underestimated in our study because of the use of 5-mm collimation. Such histologic findings of active alveolitis were seldom seen in our experience with UIP (26). In our study, patchy alveolar septal fibrosis and granulation tissue within alveoli and alveolar ducts were the major causes of slightly increased attenuation of the lung.

Patients with UIP frequently had coexisting emphysematous lesions that were seen on HRCT scans, particularly in the upper zones of the lung (Fig 7). Emphysema could be histologically distinguished from honeycombing by the presence of fibrosis around the cystic lesions. In open lung biopsy specimens, minor localized emphysematous lesions were relatively common, but extensive emphysema was recognized in only two cases. This may be the result of the surgeon's avoidance of obvious bullous involvement at biopsy sites. The present association of pulmonary emphysema and UIP is presumably related to the fact that most of our patients were smokers or ex-smokers.

High-attenuation nodules were infrequently observed on the HRCT scans. Because such nodules were complicated by the subsequent development of bronchogenic carcinoma in our series, they should be observed with care. Turner-Warwick et al have pointed out a close relationship between cryptogenic fibrosing alveolitis and bronchogenic carcinoma; in their series, 9.8% of the patients with cryptogenic fibrosing alveolitis had associated lung cancer (27). Similarly, in 12 patients with idiopathic pulmonary fibrosis studied by Müller et al, one patient had bronchogenic carcinoma

(16). In our series, bronchogenic carcinoma eventually developed in five (10.9%) of 46 cases of UIP.

In conclusion, HRCT scanning provides excellent visualization of the microscopic honeycombing and perilobular distribution of lesions in UIP. The specificity and clinical usefulness of these HRCT findings for UIP should be further investigated with prospective studies to examine a large number of cases with a variety of interstitial lung diseases. ■

References

1. Zerhouni EA, Naidich DP, Stitik FP, Khouri NF, Siegelman SS. Computed tomography of the pulmonary parenchyma. II. Interstitial disease. J Thorac Imaging 1985; 1:54–64.
2. Bergin CJ, Müller NL. CT in the diagnosis of interstitial lung disease. AJR 1985; 145: 505–510.
3. Bergin CJ, Müller NL. CT of interstitial lung disease: a diagnostic approach. AJR 1986; 148:8–15.
4. Nakata H, Kimoto T, Nakayama T, Kido M, Miyazaki N, Harada S. Diffuse peripheral lung disease: evaluation by high-resolution computed tomography. Radiology 1985; 157:181–185.
5. Itoh H, Todo G, Murata K, et al. Recent progress of chest imaging. In: Hayaishi O, Torizuka K, eds. Biomedical imaging. New York: Academic Press, 1986; 249–271.
6. Mathieson JR, Mayo JR, Staples CA, Müller NL. Chronic diffuse infiltrative lung disease: comparison of diagnostic accuracy of CT and chest radiography. Radiology 1989; 171:111–116.
7. Müller NL, Miller RR. Computed tomography of chronic diffuse infiltrative lung disease. I. Am Rev Resp Dis 1990; 142:1206–1215.
8. Murata K, Itoh H, Todo G, et al. Centrilobular lesions of the lung: demonstration by high-resolution CT and pathological correlation. Radiology 1986; 161:641–645.
9. Todo G, Herman PG. High-resolution computed tomography of the pig lung. Invest Radiol 1986; 21:689–696.
10. Nishimura K, Itoh H. Radiologic findings of patients with diffuse panbronchiolitis. In: Grassi C, Rizzato G, Pozzi E, eds. Sarcoidosis and other granulomatous disorders. Amsterdam: Elsevier Science, 1988; 747–752.
11. Webb WR, Stein MG, Finkbeiner WE, Im JG, Lynch D, Gamsu G. Normal and diseased isolated lungs: high-resolution CT. Radiology 1988; 166:81–87.
12. Murata K, Khan A, Herman PG. Pulmonary parenchymal disease: evaluation with high-resolution CT. Radiology 1989; 170: 629–635.
13. Carrington CB, Gaensler EA, Coutu RE, FitzGerald MX, Gupta RG. Natural history and treated course of usual and desquamative interstitial pneumonia. N Engl J Med 1978; 298:801–809.
14. Crystal RG, Fulmer JD, Roberts WC, Moss ML, Line BR, Reynolds HY. Idiopathic pulmonary fibrosis: clinical, histologic, radiographic, physiologic, scintigraphic, cytologic, and biochemical aspects. Ann Intern Med 1976; 85:769–788.
15. Müller NL, Miller RR, Webb WR, et al. Fibrosing alveolitis: CT-pathologic correlation. Radiology 1986; 160:585–588.
16. Müller NL, Staples CA, Miller RR, Vedal S, Thurlbeck WM, Ostrow D. Disease activity in idiopathic pulmonary fibrosis: CT and pathologic correlation. Radiology 1987; 165:731–734.
17. Westcott JL, Cole SR. Traction bronchiectasis in end-stage pulmonary fibrosis. Radiology 1986; 161:665–669.
18. Heitzman ER. The lung: radiologic-pathologic correlations. 2nd ed. St Louis: Mosby, 1984.
19. Katzenstein AA, Bloor CM, Leibow AA. Diffuse alveolar damage: the role of oxygen, shock, and related factors—a review. Am J Pathol 1976; 85:210–228.
20. Weibel ER. Looking into the lung: what can it tell us? AJR 1979; 133:1021–1031.
21. Wright PH, Buxton-Thomas M, Kreel L, Steel SJ. Cryptogenic fibrosing alveolitis: pattern of disease in the lung. Thorax 1984; 39:857–861.
22. Staples CA, Müller NL, Vedal S, Abboud R, Ostrow D, Miller RR. Usual interstitial pneumonia: correlation of CT with clinical, functional, and radiologic findings. Radiology 1987; 162:377–381.
23. Munk PL, Müller NL, Miller RR, Ostrow DN. Pulmonary lymphangitic carcinomatosis: CT and pathologic findings. Radiology 1988; 166:705–709.
24. Bergin CJ, Coblentz CL, Chiles C, Bell DY, Castellino RA. Chronic lung diseases: specific diagnosis by using CT. AJR 1989; 152:1183–1188.
25. Kitaichi M. Pathology of pulmonary sarcoidosis. Clin Dermatol 1986; 4:108–115.
26. Kitaichi M. Alveolar septal inflammation: a comparative pathological study of IPF and BOOP. In: Harasawa M, Fukuchi Y, Morinari H, eds. Interstitial pneumonia of unknown etiology. Tokyo: University of Tokyo Press, 1989; 189–199.
27. Turner-Warwick M, Lebowitz M, Burrows B, Johnson A. Cryptogenic fibrosing alveolitis and lung cancer. Thorax 1980; 35:496–499.